A Landscape Recognition Strategy Based on Polarization Characteristics of Missile-Borne Millimeter Wave Detectors

Xude Cheng, Xuedong Xue, Shuai Zhang, Wei Peng, Jian Qin

***Abstract*—To deal with the large error of burst height measurement for novel optional burst height millimeter wave proximity fuses in new-generation long-range projectiles, a ground object recognition strategy based on echo polarization is proposed in this paper. In the height measurement process, there are many factors, including the flight condition of the projectile, tall objects, ground clutter, interference signals, etc. restricting measurement accuracy. Therefore, a novel measurement scheme is urgently needed to enhance the accuracy of height measurements. The method mainly distinguishes the surface and ground objects within the range of the detected beam, under the condition that the detection area has apparent divisions. The polarimetric rotation-invariant parameters are used to analyze the features of ground objects. On the other hand, when the detection area does not have apparent divisions, the polarimetric echo reconstruction technology is used to determine the surface. Simulation experiments show the feasibility and superiority of the proposed method compared with the traditional height measurement system. Even in the presence of extensive interference, the method allows the accurate measurement of the projectile's height above the ground.**

***Index Terms*—polarization characteristics; burst height measurement; missile-borne millimeter wave detector; echo reconstruction; rotation invariant parameter**

I. Introduction

THE urgent need for precision guided weapon research and the rapid development of miniaturization microwave and millimeter wave devices and technologies have driven the study of electronic fuses, and in particular millimeter wave fuses [1]. In recent years, the complexity of battlefield environments has led to higher and higher demands on millimeter-wave fuses. In order to increase the multi-combat capability of new box-type rockets, the selection of the burst height of the proximity fuse has become a research hotspot. The millimeter wave detector antenna control and the height of burst measurement methods utilized by this type of fuses have become the key to their development.

So far, research on missile-borne millimeter-wave detectors mainly focuses on the detection signal formulation, echo signal processing, parameter estimation, etc. The relevant research results provide technical support for improving the measurement accuracy of missile-borne millimeter-wave detectors, and lay the foundation for further research. Some representative works include: SEN [2] et al. studied the target detection strategy of adaptive Orthogonal Frequency Division Multiplexing (OFDM) radars, and proposed a multi-path reflection scenario (for example, in densely-built populated areas). They used a moving target detection algorithm, which makes full use of the diversity of the Doppler shift of the echo signal during multipath propagation, and realizes the effective detection of ground moving targets. The effectiveness of their method was demonstrated through a series of numerical simulation experiments. CHEN [3] proposed an optimized waveform method for adaptive distributed multiple-input multiple-output (AD-MIMO) radar, which first extracted the Mutual Information (MI) between target echo bursts, and then minimized the MI between successive backscattered signals, so as to improve the target detection and feature extraction ability. As the number of iterations of the algorithm increased, the method could also improve the probability of target detection and Delay-Doppler resolution[4].

The above methods and strategies were based on extracting the amplitude, phase and frequency information of the signal. Under certain application conditions, target recognition and detection can be improved, but there are still some limitations, including: anti-interference ability, weak signal detection capabilities, etc. Electromagnetic waves transmitted in space are electromagnetic vector signals, which, apart from the amplitude, phase and frequency information, also contain polarization information[5]. As far as radar signals are concerned, the polarization information reflects the vector characteristics of the electromagnetic waves. It is another important datum that can be used in the time and frequency domain and propagation analysis of electromagnetic waves. Fully exploiting polarization information provides a broad space for the improvement of modern radar detection systems' performance[6]. Xiao Shunping and Wang Xuesong analyzed the superiority and feasibility of wideband polarized radar signal processing in their respective doctoral theses, and explained that the polarization information of radar signals can be used in radar signal processing[7-8]. At the same time, they revealed the great advantages of polarization information in precision guidance, sensitive array signal processing and anti-interference. Subsequently, the team analyzed in detail the electromagnetic wave transient polarization numerical description[9]. Firstly, the physical meaning of the transient Stokes vector component was described, and approximations were provided for obtaining the statistical distribution function of the instantaneous Stokes vector; secondly, under

Manuscript received Jan. 18, 2019; revised Aug. 13, 2019.

Xude Cheng is with the Department of Missile, Ordnance NCO Academy, Army Engineering University of PLA, Wuhan, 430000 China (Phone: 13871160380, e-mail: chengxd_jxsg@sina.com).

Xuedong Xue, Shuai Zhang, Wei Peng and Jian Qin are both with the Department of Missile, Ordnance NCO Academy, Army Engineering University of PLA, Wuhan, 430000 China.

the condition of Gaussian hypothesis, the analytical expression of the probability density function (PDF) of the instantaneous Stokes vector was given; the results provided theoretical support for transient polarization information processing.

With the in-depth study of polarization information processing, many experts and scholars have applied this method to different professional fields and have achieved good results. In terms of precision guidance, many target feature recognition schemes based on polarization signal processing have been proposed. LI et al. proposed a novel W-band digital variable polarization target characteristic measurement radar, which can accurately extract the target polarization scattering matrix under various polarization systems[10], and has full-polarization target Radar Cross Section (RCS) measurement capabilities. They performed an analysis and research of target polarization characteristics so as to illustrate the feasibility of polarization information applications.

This paper aims to apply polarization information measurements on a missile-borne millimeter wave radar detector, and proposes a geomorphic identification strategy for the new height of burst optional proximity fuse. This strategy mainly distinguishes between the surface and the ground objects in the range of the detection beam, and excludes the influence of dense and high ground objects on the elevation measurement of the projectile to the ground. For detection areas with obvious discrete features, round objects are analyzed using the polarization rotation invariant parameter; for detection areas without obvious features, the polarization echo reconstruction technique is used for this determination.

II. Polarization Rotation-Invariant Parameter Target Recognition

The receiving end of the missile-borne millimeter wave detector uses a dual-polarized instantaneous synchronous receiving mode of operation. Then, the antenna array transmits signal $\boldsymbol{s}(t)$, which can be expressed as:

$$\boldsymbol{s}(t)=\begin{bmatrix} s_1(t) & s_2(t) & \ldots & s_N(t)\end{bmatrix}^{\mathrm{T}} \quad (1)$$

In equation (1), N is the number of array elements, while T indicates transposition. It is assumed that the ground environment within the detection range has stable polarization scattering characteristics at the operating frequency. Then, its scattering properties can be characterized by a polarization scattering matrix $\boldsymbol{S}$:

$$\boldsymbol{S}=\begin{bmatrix} S_{\mathrm{HH}} & S_{\mathrm{HV}} \\ S_{\mathrm{VH}} & S_{\mathrm{VV}}\end{bmatrix}=\begin{bmatrix} |S_{\mathrm{HH}}|e^{j\varphi_{\mathrm{HH}}} & |S_{\mathrm{HV}}|e^{j\varphi_{\mathrm{HV}}} \\ |S_{\mathrm{VH}}|e^{j\varphi_{\mathrm{VH}}} & |S_{\mathrm{VV}}|e^{j\varphi_{\mathrm{VV}}}\end{bmatrix} \quad (2)$$

In (2), the subscript $mn(m,n=\mathrm{H,V})$ indicates polarization transmission from n to polarization reception from m; H is the horizontal polarization mode and V is the vertical polarization mode. Since the missile-borne array antennae of millimeter-wave detectors are shared, the horizontal and vertical polarization components of the received signal at the first array element can be expressed as:

$$\boldsymbol{x}_{k\,\mathrm{HH}}(t)=\sqrt{P_r}\cdot\boldsymbol{\alpha}(\theta)\cdot\boldsymbol{s}(t-\tau)\cdot S_{\mathrm{HH}}\cdot e^{j2\pi f_d t}\cdot g(k,\theta) \quad (3)$$

$$\boldsymbol{x}_{k\,\mathrm{HV}}(t)=\sqrt{P_r}\cdot\boldsymbol{\alpha}(\theta)\cdot\boldsymbol{s}(t-\tau)\cdot S_{\mathrm{HV}}\cdot e^{j2\pi f_d t}\cdot g(k,\theta) \quad (4)$$

$$\boldsymbol{x}_{k\,\mathrm{VH}}(t)=\sqrt{P_r}\cdot\boldsymbol{\alpha}(\theta)\cdot\boldsymbol{s}(t-\tau)\cdot S_{\mathrm{VH}}\cdot e^{j2\pi f_d t}\cdot g(k,\theta) \quad (5)$$

$$\boldsymbol{x}_{k\,\mathrm{VV}}(t)=\sqrt{P_r}\cdot\boldsymbol{\alpha}(\theta)\cdot\boldsymbol{s}(t-\tau)\cdot S_{\mathrm{VV}}\cdot e^{j2\pi f_d t}\cdot g(k,\theta) \quad (6)$$

In equations (3) to (6), P_r is the antenna power gain coefficient; f_d is the Doppler frequency shift; $\boldsymbol{\alpha}(\theta)$ is the antenna transmission steering vector function; $g(k,\theta)$ is the angle component function when the k^{th} array element receives the signal, and $g(k,\theta)=\exp[j2\pi(k-1)d\sin\theta/\lambda]$. For a missile-borne millimeter-wave detector, the received horizontal and vertical polarization components can be expressed as:

$$\boldsymbol{x}_{\mathrm{HH}}(t)=\sqrt{P_r}\cdot\boldsymbol{\alpha}(\theta)\cdot\boldsymbol{\beta}(\theta)\cdot\boldsymbol{s}(t-\tau)\cdot S_{\mathrm{HH}}\cdot e^{j2\pi f_d t} \quad (7)$$

$$\boldsymbol{x}_{\mathrm{HV}}(t)=\sqrt{P_r}\cdot\boldsymbol{\alpha}(\theta)\cdot\boldsymbol{\beta}(\theta)\cdot\boldsymbol{s}(t-\tau)\cdot S_{\mathrm{HV}}\cdot e^{j2\pi f_d t} \quad (8)$$

$$\boldsymbol{x}_{\mathrm{VH}}(t)=\sqrt{P_r}\cdot\boldsymbol{\alpha}(\theta)\cdot\boldsymbol{\beta}(\theta)\cdot\boldsymbol{s}(t-\tau)\cdot S_{\mathrm{VH}}\cdot e^{j2\pi f_d t} \quad (9)$$

$$\boldsymbol{x}_{\mathrm{VV}}(t)=\sqrt{P_r}\cdot\boldsymbol{\alpha}(\theta)\cdot\boldsymbol{\beta}(\theta)\cdot\boldsymbol{s}(t-\tau)\cdot S_{\mathrm{VV}}\cdot e^{j2\pi f_d t} \quad (10)$$

In equations (17) to (20), $\boldsymbol{\beta}(\theta)$ is the steering vector function of antenna reception. For a missile-borne millimeter-wave detector (which can be regarded as a single-station radar), we have $\boldsymbol{\alpha}(\theta)=\boldsymbol{\beta}(\theta)$. It can be seen from the above derivation process that the antenna array can acquire the target polarization scattering characteristics, which lays the foundation for target recognition.

In the process of measuring the elevation over the ground, it is necessary to identify the ground objects in the range of the probe beam. Therefore, the target features of the object have become the focus of attention. Because the angle between the projectile and the ground object is uncertain during the flight of the rocket, the polarization target is used to identify the ground object[11].

If the dissimilarity theorem holds, then the polarization scattering matrix $\boldsymbol{S}$, S_{HV} and S_{VH} can be regarded as equal, and according to matrix theory, there must be some invertible matrix $\boldsymbol{P}$, such that the scattering matrix $\boldsymbol{S}$ can be diagonalized, i.e.:

$$\boldsymbol{P}^{-1}\boldsymbol{S}\boldsymbol{P}=\begin{bmatrix}\lambda_1 & \omega \\ 0 & \lambda_2\end{bmatrix} \quad (11)$$

In equation (11), λ_1 and λ_2 are the eigenvalues of the scattering matrix. Then, the value of ω can only be 0 or 1. When $\omega=0$, λ_1 and λ_2 have a set of orthogonal eigenvectors; when $\omega=1$, $\lambda_1=\lambda_2$.

Then, when the angle between the target and the detector changes within the detection range, the corresponding scattering matrix can be expressed as:

$$\boldsymbol{S}(\psi)=\boldsymbol{J}(\psi)\cdot\boldsymbol{S}\cdot\boldsymbol{J}(-\psi) \quad (12)$$

In equation (12), the rotation matrix can be expressed as:

$$\boldsymbol{J}(\psi)=\begin{bmatrix}\cos\psi & -\sin\psi \\ \sin\psi & \cos\psi\end{bmatrix} \quad (13)$$

It is easy to prove that $\boldsymbol{J}(-\psi)=\boldsymbol{J}^{-1}(\psi)$, so it is available:

$$[\boldsymbol{J}(\psi)\cdot\boldsymbol{P}]^{-1}\cdot\boldsymbol{S}\cdot[\boldsymbol{J}(\psi)\cdot\boldsymbol{P}]=\begin{bmatrix}\lambda_1 & \omega \\ 0 & \lambda_2\end{bmatrix} \quad (14)$$

It can be seen from equation (14) that when the scattering matrix is rotated by an angle ψ, the new scattering matrix has the same upper triangular matrix as the original, so it can be used as the rotation-invariant parameter for the next analysis.

According to the conclusion in [12], any target polarization scattering matrix can be represented by a linear

combination of three standard bodies' (planar, dihedral, spirochete) scattering matrices. The scattering matrices of the three standard bodies can be expressed as:

$$\boldsymbol{S}_B = \begin{bmatrix} 1 & 0 \\ 0 & 1 \end{bmatrix} \tag{15}$$

$$\boldsymbol{S}_{DA} = \begin{bmatrix} 1 & 0 \\ 0 & -1 \end{bmatrix} \tag{16}$$

$$\boldsymbol{S}_{Rl} = \begin{bmatrix} 1 & j \\ j & -1 \end{bmatrix} \quad \boldsymbol{S}_{Rr} = \begin{bmatrix} 1 & -j \\ -j & -1 \end{bmatrix} \tag{17}$$

As can be seen from equations (15) to (17), the rotation matrix includes a left-handed matrix $\boldsymbol{S}_{Rl}$ and a right-handed matrix $\boldsymbol{S}_{Rr}$. Any target scattering matrix can be expressed as:

$$\boldsymbol{S} = \xi_1 \cdot \boldsymbol{S}_B + \xi_2 \cdot \boldsymbol{S}_{DA} + \xi_3 \cdot \boldsymbol{S}_R \tag{18}$$

In equation (18), $\xi_i (i = 1,2,3)$ is the coefficient of the scattering matrix for each standard body and can be regarded as the projection distance of the target scattering matrix under a group of bases composed of $\boldsymbol{S}_B$, $\boldsymbol{S}_{DA}$ and $\boldsymbol{S}_R$. According to (14), the rotation scattering matrix contains three elements, and in order to measure the difference between different scattering matrices, a similarity measure vector is defined[15]:

$$\boldsymbol{k} = \begin{pmatrix} \lambda_1, & \lambda_2, & x \end{pmatrix}^{\mathrm{T}} \tag{19}$$

In (19), different scattering matrices have different metric matrices $\boldsymbol{k}$, as $x = \omega \cdot \sqrt{\left|S_{\mathrm{HH}}\right|^2 + 2\left|S_{\mathrm{HV}}\right|^2 + \left|S_{\mathrm{VV}}\right|^2}$. The metric vector of the standard body scattering matrix is solved as:

$$\begin{cases} \boldsymbol{k}_1 = \begin{pmatrix} 1 & 1 & 0 \end{pmatrix}^{\mathrm{T}} \\ \boldsymbol{k}_2 = \begin{pmatrix} 1 & -1 & 0 \end{pmatrix}^{\mathrm{T}} \\ \boldsymbol{k}_3 = \begin{pmatrix} 0 & 0 & 1 \end{pmatrix}^{\mathrm{T}} \end{cases} \tag{20}$$

We assume two different scattering matrices $\boldsymbol{S}_1$ and $\boldsymbol{S}_2$ and their corresponding metric matrices respectively, and define the projection distance to solve the expression:

$$dis\begin{pmatrix} \boldsymbol{S}_1 & \boldsymbol{S}_2 \end{pmatrix} = \frac{\left| \left(\boldsymbol{k}_1^* \right)^{\mathrm{T}} \cdot \boldsymbol{k}_2 \right|^2}{\left\| \boldsymbol{k}_1 \right\|_2^2 \cdot \left\| \boldsymbol{k}_2 \right\|_2^2} \tag{21}$$

In (21), $\| \ \|_2$ represents the vector -2 norm. Then, the correlation coefficient in (8) can be expressed as:

$$\begin{cases} \xi_1 = dis\begin{pmatrix} \boldsymbol{S} & \boldsymbol{S}_B \end{pmatrix} \\ \xi_2 = dis\begin{pmatrix} \boldsymbol{S} & \boldsymbol{S}_{DA} \end{pmatrix} \\ \xi_3 = dis\begin{pmatrix} \boldsymbol{S} & \boldsymbol{S}_R \end{pmatrix} \end{cases} \tag{22}$$

Therefore, the projection distances of the three standard volume scattering matrices are used to analyze the features of the objects in the detection area and to extract the ground objects from the ground to achieve target recognition.

III. Polarization Signal Reconstruction Recognition Technology

When the target object density in the detection area is low, the polarization rotation-invariant parameter identification method can distinguish the echo signals of the ground and the objects effectively. However, when the local object concentration is high, most of the echo signals are composed of high-ground echoes[12], and the ground echo is embedded in them, which complicates the determination of the polarization rotation-invariant parameters of the echo signals. Therefore, in this paper we use reconstructed echo signal analysis to deal with the severe suppression interference (higher target density) and extract ground and ground echo information.

It can be seen from the second section that the echo signals from the ground and the ground objects intercepted by the detector antenna contain polarization characteristics, and the beam outputs formed by the horizontally and vertically polarized channels can be respectively expressed as[16]:

$$\boldsymbol{y}_{\mathrm{V}} = \left| \boldsymbol{y}_{\mathrm{V}} \right| \cdot \exp(j\phi_{\mathrm{V}}) \tag{23}$$

$$\boldsymbol{y}_{\mathrm{H}} = \left| \boldsymbol{y}_{\mathrm{H}} \right| \cdot \exp(j\phi_{\mathrm{H}}) \tag{24}$$

In equations (13) and (14), $\left| \ \right|$ is the energy of the echo signal. Then, at sample n, the normalized elements in the transient Stokes polarization vector of the echo signal can be expressed as:

$$\overline{g}_1 = \frac{\left| y_{\mathrm{H}}(n) \right|^2 - \left| y_{\mathrm{V}}(n) \right|^2}{\left| y_{\mathrm{H}}(n) \right|^2 + \left| y_{\mathrm{V}}(n) \right|^2} \tag{25}$$

$$\overline{g}_2 = \frac{2\left| y_{\mathrm{H}}(n) \right| \cdot \left| y_{\mathrm{V}}(n) \right| \cdot \cos(\phi_{\mathrm{V}} - \phi_{\mathrm{H}})}{\left| y_{\mathrm{H}}(n) \right|^2 + \left| y_{\mathrm{V}}(n) \right|^2} \tag{26}$$

$$\overline{g}_3 = \frac{2\left| y_{\mathrm{H}}(n) \right| \cdot \left| y_{\mathrm{V}}(n) \right| \cdot \sin(\phi_{\mathrm{V}} - \phi_{\mathrm{H}})}{\left| y_{\mathrm{H}}(n) \right|^2 + \left| y_{\mathrm{V}}(n) \right|^2} \tag{27}$$

The Stokes vector obtained from equations (25) to (27) can be expressed as $\overline{\boldsymbol{g}} = (\overline{g}_1 \quad \overline{g}_2 \quad \overline{g}_3)^{\mathrm{T}}$.

In the previous work, it is possible to measure the ground-scattered normalized Stokes vector in a certain pulse, and set its value (Stokes vector $\overline{\boldsymbol{g}}_{act}$) as the prior knowledge of the fuse detector at the beginning of the launch. We then contrast with real-time measurement vectors to identify the ground and features within the detection area. We define the similarity measure function as[17]:

$$D = \arccos(\overline{\boldsymbol{g}}^{\mathrm{T}} \cdot \overline{\boldsymbol{g}}_{act}) \tag{28}$$

In (28), D is the similarity result between the two Stokes vectors. In the actual signal processing process, when the target echo and interference signals can be distinguished in distance, even if the intensity of the interference signal severely suppresses the target signal, the polarization recognition method can be used to detect the distance unit of the target echo signal effectively and to mitigate the effects of strongly interfering echo signals.

IV. Simulation Experiment

In this paper, we used the FEKO software to model to simulate the proposed polarization height measurement strategy. FEKO is a professional electromagnetic field analysis software developed for electromagnetic compatibility analysis, RCS analysis, etc. It can solve electromagnetic simulation problems of complex structures easily and quickly [13].

When modeling with FEKO, the solution process is not limited by the geometry of the object. Theoretically, any object shape can be modeled, which is conducive to accurate modeling of complex and irregular objects. The modeling method is simple. The FEKO CAD module provides a complete graphical tool for geometric modeling. The geometric language modeling method makes the model establishment simple and fast.

We modeled two typical ground environments: bare land (i.e. mostly low plants within the detection range, close

to the ground) and dense groves (mainly tall trees within the detection range). Typical examples of such landscapes are shown in Figure 5:

(1) Real scene of approximately bare land

(2) Real scene of dense grove landscape

Fig. 5 Typical topography landscapes

As shown in Fig. 5, a dense open lawn was selected as the research object, and the measured grass height was about 1-10 cm, almost windless, with a lawn coverage rate of more than 80%. An evergreen small leafy dense grove was selected as the second research object, where the measured tree height was about 1-2 m and the trunk diameter was 5-10 cm. The geomorphological features shown in Fig. 5(1) were established in the FEKO CAD module, and plane wave excitation was added in the longitudinal direction, so that the emitted electromagnetic waves were horizontally and vertically polarized. The backscattering results shown in Fig. 6 were obtained.

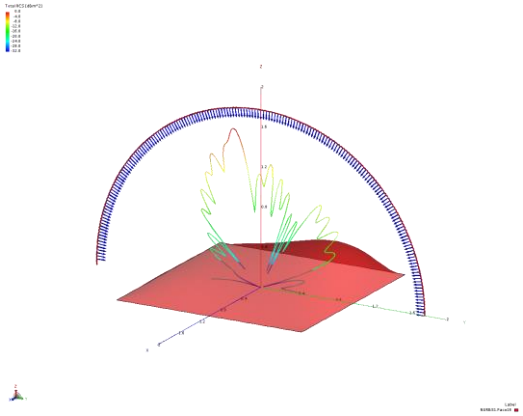

(1) Surface backscatter measurements using horizontally polarized plane wave

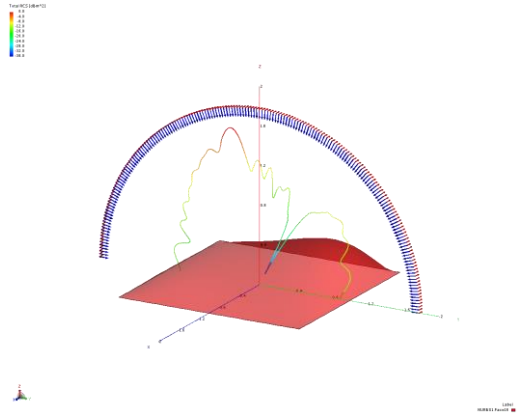

(2) Surface backscatter measurements using vertically polarized plane wave

Fig. 6. Backscatter measurement results of bare land landscape with horizontally and vertically polarized plane waves.

Using the output of the *.ffe file, the amplitudes of the different polarizations (HH, VV, VH, HV) of the echoes can be obtained. The normalized amplitudes of the four polarization modes obtained after processing are shown in Figure 7.

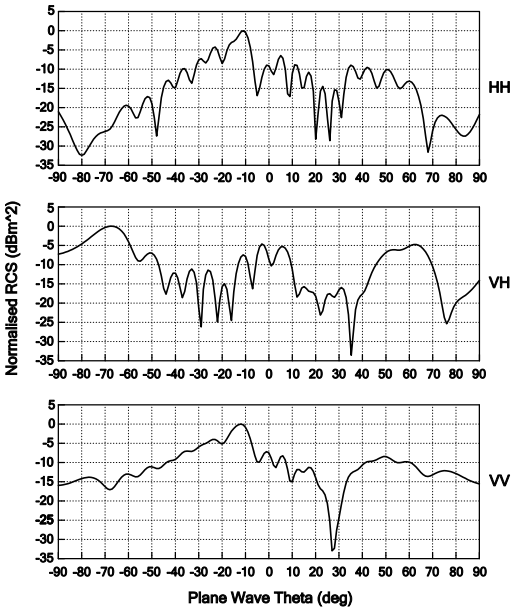

Fig. 7. Backscatter results of bare land under the different polarized styles

Since the backscattering results obtained by the VH and HV polarization modes are the same, only the values obtained in the VH polarization mode are shown. The flight path of the rocket projectile was designed, and a set of polarization measurement values of a certain angle were considered to obtain the scattering matrix. Finally, the determination result shown in Table I was obtained.

TABLE I
CALCULATION RESULTS OF PROJECTION DISTANCE OF APPROXIMATELY BARE LAND LANDSCAPE

Angle	ξ_1	ξ_2	ξ_3	Recognition Results
-30°	0.8966	0.1034	0	Surface reflection
-20°	0.8994	0.1006	0	Surface reflection
-10°	0.3904	0.6096	0	Dihedral surface reflection
0°	0.5214	0.4786	0	Surface reflection
10°	0.5674	0.4326	0	Surface reflection
20°	0.5365	0.4635	0	Surface reflection
30°	0.6232	0.3768	0	Surface reflection

As can be seen from Table 1, the results measured at the above angles are closest to the plane scattering characteristics (the correlation coefficient value is the largest), and therefore they can be determined as surface reflection. When the missile-borne millimeter wave detector operates between -30° and 30°, it has the ability to identify the approximately bare land, with a recognition rate of 85.71%. Similarly, a dense grove model was built on the surface model, and modeled in the FEKO CAD module according to a certain ratio. The results are shown in Fig. 8.

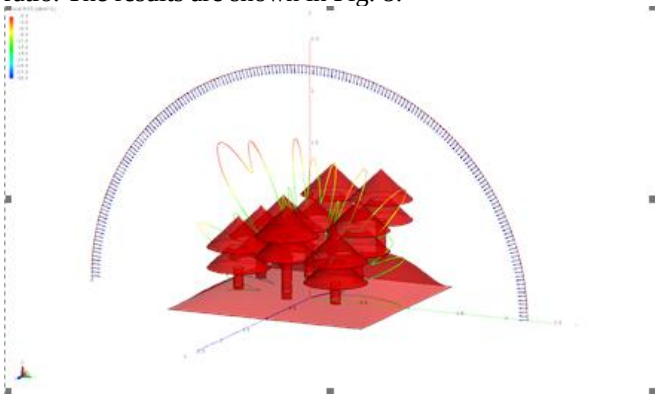

(1) Ground object target backscatter measurements using horizontally polarized plane waves

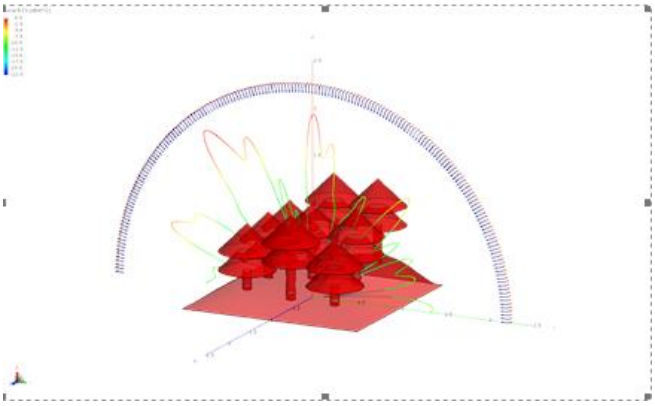

(2) Ground object target backscatter measurements using vertically polarized plane waves

Fig. 8. Backscatter measurement results of dense grove landscape with horizontally polarized plane wave and vertical polarized plane wave

Similarly to the bare land experiment, the resulting *.ffe file was processed to obtain the normalized amplitude results of the four polarization modes in the case of dense groves. The results are shown in Fig. 9.

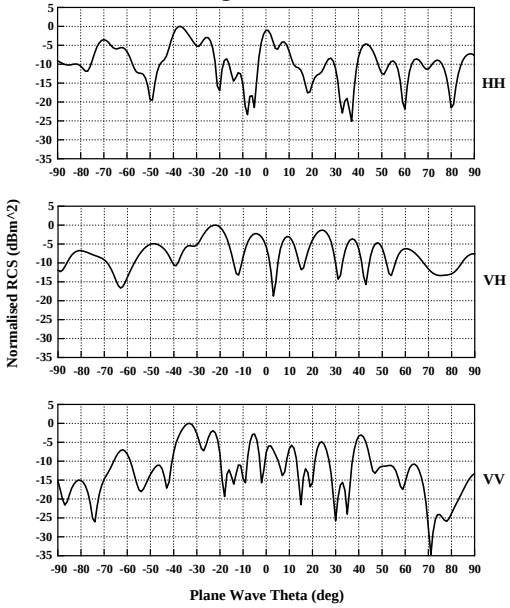

Fig. 9. Backscatter results of dense grove under the different polarized modes

Similarly, the scattering matrix was obtained under the condition of dense groves, and the results were further processed, as shown in Table 2.

TABLE II
CALCULATION RESULTS OF PROJECTION DISTANCE OF DENSE GROVE LANDSCAPE

Angle	ξ_1	ξ_2	ξ_3	Recognition result
-30°	0.3586	0.6414	0	Dihedral surface reflection
-20°	0.8855	0.1145	0	Surface reflection
-10°	0.7646	0.2354	0	Surface reflection
0°	0.2930	0.7070	0	Dihedral surface reflection
10°	0.1873	0.8127	0	Dihedral surface reflection
20°	0.0572	0.7428	0	Dihedral surface reflection
30°	0.3273	0.6727	0	Dihedral surface reflection

As can be seen from the table, the measurement results at the above angle is closest to the dihedral angle scattering characteristic (the correlation coefficient value is the largest), and therefore they can be determined as surface reflection. The missile-borne millimeter-wave detector has the ability to identify dense woodland when operating between -30° and 30°, with a recognition rate of 71.43%.

Further, polarization signal reconstruction was performed on the above simulation result data, and the Stokes vector of the two topographic features was solved using the solution result in the *.ffe file to increase the measurement accuracy at a specific angle. The Stokes vectors obtained from the bare land and the dense grove are shown in Table 3.

TABLE III
STOKES VECTOR RESULTS OF BARE LAND LANDSCAPE AND DENSE GROVE LANDSCAPE, AND THEIR APPROXIMATION

Angle (°)	Bare land		
	$\bar{g}_1$	$\bar{g}_2$	$\bar{g}_3$
-30	0.0088	0.9766	-0.2148
-20	-0.1929	0.9310	-0.3099
-10	0.2330	0.9697	0.0731
0	0.0024	0.9999	-0.0151
10	0.5591	0.5203	-0.6455
20	-0.8899	0.3770	0.2567
30	0.7086	0.6967	0.1116
Angle (°)	Dense grove		
	$\bar{g}_1$	$\bar{g}_2$	$\bar{g}_3$
-30	0.3547	0.8197	-0.4497
-20	0.3323	0.3773	0.8644
-10	0.2063	0.7351	0.6459
0	-0.5924	0.8028	0.0684
10	0.1075	0.9234	0.3686
20	0.4525	0.5803	-0.6771
30	-0.7808	-0.1167	0.6138

Angle (°)	Similar degree D	Result
-30	0.4504	Ground
-20	1.5515	Not ground
-10	0.6299	Ground
0	0.6432	Ground
10	1.2634	Not ground
20	1.9366	Not ground
30	2.1725	Not ground

Through the calculation of the Stokes vector and the similarity solution, the millimeter wave detector has the ability to recognize the surface and the ground objects, and this illustrates the effectiveness of the proposed terrain identification strategy. Compared with traditional millimeter wave fuses, this strategy provides the ability to identify geomorphological features, improving measurement accuracy and anti-interference ability.

Different polarization combinations can be used to obtain different recognition results. According to the above experimental results, the recognition accuracy can reach the high levels required for preset missions. After a series of actual experiments, the recognition accuracy reached nearly 90%. The recognition method has been used in novel missile-borne detectors and the difference between different landscapes was distinguished.

Meanwhile, a series of tests were conducted to demonstrate the superiority of the proposed recognition algorithm. The results are shown in Fig. 10.

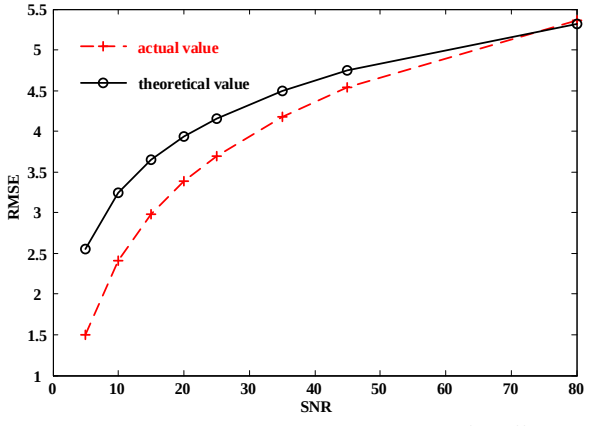

(a)

comparison between actual value and theoretical value for different SNRs

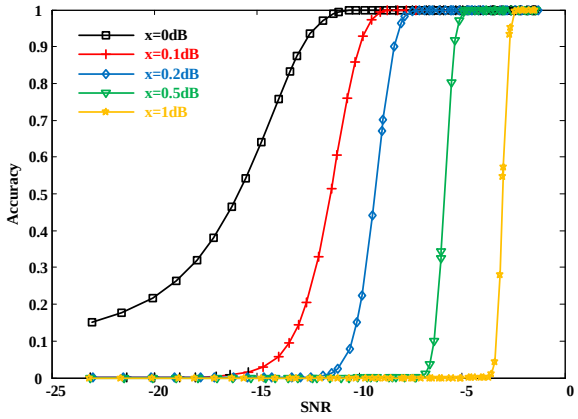

(b) accuracy of different noise uncertainties for different SNRs.

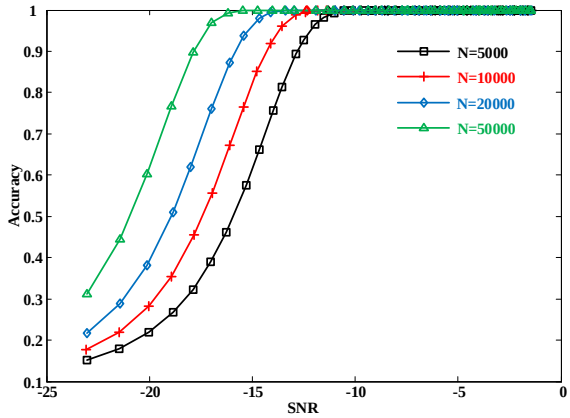

(c) accuracy for different numbers of sampling points in different SNRs

Fig. 10 Simulation results for algorithm performance verification

Fig. 10(b) shows the relationship between the detection probability of energy detection and SNR when the noise uncertainty is 0, 0.5, 0.7 and 1 dB, respectively. It can be seen from the curve that the noise uncertainty is only 0.1dB. When the detection probability is 0.9, the detection performance of energy detection decreases by 3.5dB. When the noise uncertainty reaches 1dB, the detection performance decreases by about 10dB compared with that when the noise power is determined.

Compared with conventional recognition algorithms, the proposed algorithm has better recognition accuracy and higher efficiency. In fig. 10(b) and 10(c), with the gradual increase of SNR and of the number of sampling points, the algorithm converges faster. These comparative tests illustrate the advantages of the recognition algorithm proposed in this paper. Fig. 10(b) and 10(c) show the relationship between detection probability and SNR under different sampling points when the energy detection method has no noise uncertainty and the noise uncertainty is 0.5dB, respectively. When the sampling points are 5000, 10000, 20000, 50000 respectively, the detection probability increases obviously with the increase of sampling points, and when the noise uncertainty is 0.5dB. The detection performance does not increase with the increase of sampling points. The testing performance is obviously improved. In the actual spectrum detection process, there is some uncertainty in the noise power, and the detection performance of energy detection cannot be significantly improved by increasing the sampling points.

V. Conclusion

To deal with the problem of large height measurement errors of the new missile-borne millimeter wave detectors, this paper proposes a feature recognition strategy based on polarization features, which enables the detector to actively resolve the ground surface and tall ground objects during the height measurement process, and avoid the effect of strong interference of tall ground objects. The analysis of polarization rotation-invariant parameters is proposed for target recognition. The polarization echo signal intercepted by the missile-borne millimeter wave detector is projected onto the rotation-invariant scattering matrix of three standard bodies to determine the obtained projection distance as a basis for recognition, and it is possible to recognize the ground surface and tall ground objects effectively. The polarization signal reconstruction method is used to further process the echo signals of the complex geomorphological environment, and the distance of the target echo signal is detected effectively, thereby invalidating the effect of the strong interference echo signal. Finally, the above strategy is simulated using the FEKO simulation software, and the effectiveness and superiority of the strategy are verified.

References

[1] D. K. Wu, “The research of some key technologies and application in miniature millimeter wave fuse”. Chengdu: University of Electronic Science and Technology of China, 2010.

[2] S. Sen and A. Nehorai. (2011) “Adaptive OFDM radar for target detection in multipath scenarios”. *IEEE Transactions on Signal Processing*, 59(1): pp. 78-90.

[3] Y. F. Chen, Y. Nijsure, C. Yuen, et al. (2013) “Adaptive distributed MIMO radar waveform optimization based on mutual information”. *IEEE Transactions on Aerospace and Electronic Systems*, 49(2): pp. 1374-1385.

[4] S. Zheng, X. H. Pan, A. X. Zhang, et al. (2015) “Estimation of echo amplitude and time delay for OFDM based ground penetrating radar”. *IEEE Geoscience and Remote Sensing Letters*, 12(12): pp. 2384-2388.

[5] L. Z. Song and X. L. Qiao. (2013) “Research on key techniques of a polarized MIMO radar seeker”. *Transactions of Beijing Institute of Technology*, 33(6): pp. 644-649.

[6] D. H. Dai, B. Liao, S. P. Xiao, et al. (2016) “Advancements on radar polarization information acquisition and processing”. *Journal of Radars*, 5(2): pp. 148-165.

[7] S. P. Xiao, “Study on wideband polarimetic radar target recognition”. Changsha: National University of Defense Technology, 1995.

[8] X. S. Wang, “Study on wideband polarization information processing”. Changsha: National University of Defense Technology, 1999.

[9] X. S. Wang, Y. Z. Li, D. H. Dai, et al. (2004) “Instantaneous polarization statistics of electromagnetic waves”. *Science in China Series F*, 47(5): pp. 623-634.

[10] Z. F. Li, B. Hu, G. Q. Zhao, et al. (2017) “A W-band digital variable polarimetric radar for target characteristic measurement”. *J. Infrared Millim. Waves*, 36(1): pp. 35-41.

[11] T. Y. Lu, J. Yi, Q. L. Xia, et al. (2015) “A kind of decoupling algorithm of phased array seeker based on beam angle error compensation”. *Systems Engineering and Electronics*, 37(9): pp. 2123-2128.

[12] Y. P. Cheng, K. Y. Zhang, and Z. Xu. “*Matrix theory*”. Xi’an: Northwestern Polytechnical University Press, 2013.

[13] E. Krogager. (1990) “New decomposition of the radar target scattering matrix”. *Electronics Letters*, 26(8): pp. 1525-1527.

[14] T. Taniguchi, M. Sugeno. (2018) “Trajectory tracking controls for non-holonomic systems using dynamic feedback linearization based on piecewise multi-linear models”. *International Journal of Applied Mathematics*, 47(3): pp. 339-351.

[15] I. C. Demetriou. (2013) “An application of best L1 piecewise monotonic data approximation to signal restoration”. *International Journal of Applied Mathematics*, 47(4): pp. 226-232.

[16] B. Jonathan, B. Bazar. (2013) “Three-dimensional simulation of the field patterns generated by an integrated antenna”. *IAENG International Journal of Applied Mathematics*, 43(3): pp. 138-153.

[17] B. B. Firouzi, T. Niknam, M. Nayeripour. (2009) “A new evolutionary algorithm for cluster analysis”. *International Journal of Computer Science*, 4(4): pp. 605-609.